GAS-FILLED POSITION-SENSITIVE THERMAL NEUTRON DETECTOR

V.A. Andreev, G.A. Ganzha, E.A. Ivanov, D.S. Ilyin, L.M. Kochenda, S.N. Kovalenko, M.R. Kolkhidashvili, A.G. Krivshich, A.V. Nadtochy, A.I. Okorokov, V.V. Runov, G.D. Shabanov, V.A. Solovei

1. Introduction

Multi-wire proportional chambers filled with the ^{3}He + CF$_4$ gas mixture with a delay line readout are widely used for thermal neutron detection, especially in Small-Angle Neutron Scattering (SANS) instruments [1–3]. The purpose of the discussed work was to find a set of strongly interrelated detector design parameters with the aim to improve the detector performance. After careful consideration of important detector parameters, such as the space resolution, the efficiency and differential and integral nonlinearity, a satisfactory solution was found. In order to guarantee a reliable and optimal operation of the neutron detector, a wide range of scientific and technological investigations was carried out to:

- improve and optimize the detector mechanical characteristics, simulations of the detector pressure behavior up to 10 bar were performed;
- minimize the detector outgassing, a new technology for fabrication of the detector electrodes was successfully developed. It has opened a way to improve the gas purity by a few orders of magnitude;
- minimize the gas leakage to a level smaller than 0.03 % per day, the detector gas sealing technology was improved.

This paper describes general approaches and technological solutions that have allowed us to develop thermal neutron detectors for the SANS diffractometers "Vector" and "Membrana-2" at the VVR-M reactor of PNPI. The required parameters of the detector are listed in Table 1.

Table 1

The required characteristics of 2D-detectors

Characteristic	Diffractometer	
	"Membrana-2"	"Vector"
Neutron wave length, Å	3	9
Entrance window $X \times Y$, mm^2	200×200	300×300
Neutron efficiency, %	≥ 70	≥ 70
Position resolution $X \times Y$, mm^2	2×2	2×2
Counting capability, kHz	≤ 100	≤ 100
Intrinsic noise, Hz	< 0.5	< 0.5
Life time, years	≥ 5	≥ 5

2. Detector design principles

2.1. Thermal neutron detection

Neutrons are detected by their capture in the ^{3}He gas according to the nuclear reaction

$$^3\text{He} + n \rightarrow p + {}^3\text{H} + 764 \text{ keV}. \tag{1}$$

Achieving the highest detector efficiency was one of the first problems to be solved by detector construction. From this point of view, ^{3}He is very convenient gas to use because it has a large cross-section for capture of thermal neutrons, 26500 b for 9 Å neutrons.

2.2. Detector construction

Several model calculations (ANSYS 8.1) of different versions of the mechanical design of the neutron detector have been carried out using the finite-element method. The most successful design was chosen from the point of view of minimal deformations of the entrance window under internal pressure. The chamber

prototype was constructed from the aluminum alloy AMg5. This alloy has the most suitable combination of the mechanical strength and good neutron transmission properties. Moreover, as it was measured, this material has a minimal cross section for neutron small-angle scattering compared to other investigated materials for detector construction.

To ensure uniformity of the detector efficiency across the detector entrance window, it was necessary to avoid deformations of the entrance window under gas pressure. After improvements of the detector design it became possible to minimize deformations of the entrance window (of 10 mm thickness) to 0.2 mm.
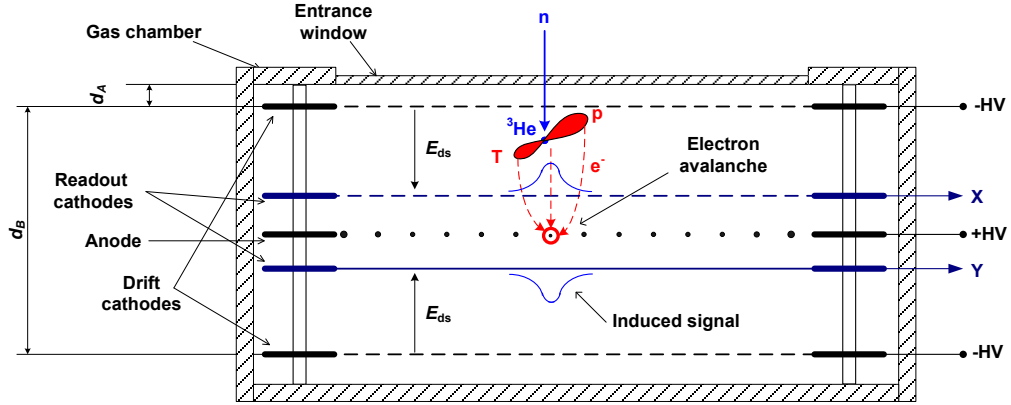

Fig. 1. Schematic diagram of the 2D-detector: E_{dr} – direction of the electric field in the drift gaps, $d_A = 1.5$ mm – the gap between the entrance window and the plane delimiting the detector sensitive volume (detector insensitive zone), $d_B = 32$ mm – the thickness of the sensitive volume, +HV and –HV – the potentials applied to the anode and the drift electrodes, respectively

The detector design (Fig. 1) was based on a Multi-Wire Proportional Chamber (MWPC). It has a conventional design with two orthogonal cathode grids symmetrically located about the central anode grid. The anode consists of gold plated tungsten wires with the diameter 25 μm, the wire spacing being $S = 4$ mm. The anode-cathode distance is $L_c = 4$ mm. The cathode wires diameter is 55 μm, the wire spacing is 1 mm. Every three wires are connected together into one strip, which is connected to a delay line with an impedance of 100 Ohm with a specific delay of 6 ns per strip. So, the strip pitch is $w = 3$ mm. In order to increase the detector efficiency, there were two 12 mm absorption/drift regions, which were adjacent to both cathodes of the MWPC. In this way, the detector active thickness was 32 mm.

In order to achieve the best physical parameters of the detector, it was necessary to optimize the anode signal transmission to cathode strips. For this purpose, some other geometrical parameters of the MWPC were selected close to the optimum condition: $w/L_c \approx 0.8$, which provided both high amplitude of signals induced on the cathode, Q_c, and a minimal level of the differential nonlinearity.

Because of a high cost of the ^{3}He gas, much attention was paid to the problem of gas leakage from the chamber volume. At the stage of the detector design, significant efforts were undertaken to decrease the gas leakage. To evaluate the final value of this parameter, the temperature and pressure of the gas mixture were measured in the chamber during a period of about 400 days. The time dependence of the relative density of the gas mixture was calculated. It was shown that the leakage rate was about 0.03 % per day.

2.3. Neutron efficiency

The efficiency of a neutron detector is determined by a set of factors such as the partial pressure of ^{3}He, the construction and material of the gas chamber, the geometry of the MWPC, and its location in the chamber. Special attention was paid to inevitable losses of neutrons both in the entrance window and in the intermediate gas gap between the entrance window and the first drift cathode (Fig. 1). The efficiency of the detector was calculated as

$$\varepsilon = \exp(-\mu_{Al}d_{Al}) \times \exp(-\mu_A d_A) \times [1 - \exp(-\mu_B d_B)], \tag{2}$$

where $\mu = n \times \sigma$; n is the gas atomic concentration, σ is the neutron capture cross-section, d_{Al} is the entrance window thickness, d_A is the gap thickness between the entrance window and the upper drift cathode, d_B is the thickness of the detector active area.
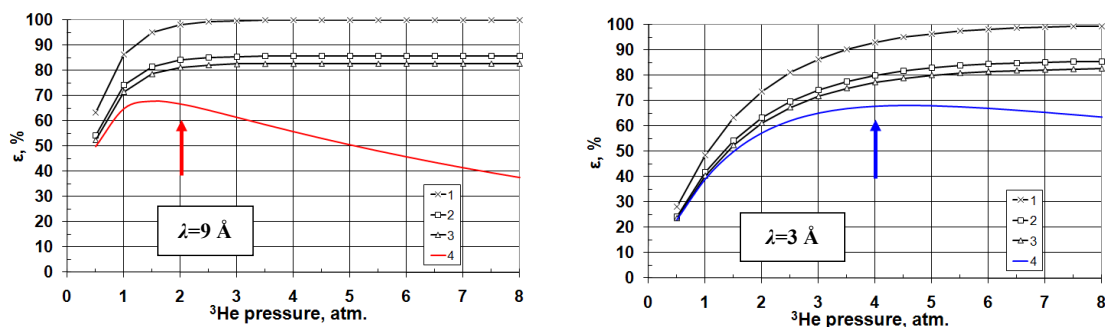

Fig. 2. Calculated efficiencies of the neutron detectors for the spectrometers "Vector" (left) and "Membrana-2" (right). (1) – neutron conversion efficiency without attenuation factors; (2) – the same as (1) with neutron losses in the entrance window; (3) – the same as (2) with losses in the upper drift electrode; (4) – the same as (3) with losses in the gap between the entrance window and the sensitive volume. This is the final detector efficiency

To achieve the required efficiency $\varepsilon \geq 70\ \%$ (Table 1), the gap between the entrance window and the upper drift cathode was reduced to $d_A = 1.5$ mm. The drift electrode was made of thin (2.5 mm) plane of quartz glass with metallic coating 15 μm thick.

The detectors were designed for different wavelengths of neutrons. The 2D-detector for the diffractometer "Vector" ($< \lambda > = 9$ Å) has achieved efficiency $\varepsilon \approx 70\ \%$ at the partial ^{3}He pressure $P(^3\text{He}) = 2$ bar, and the 2D-detector for the diffractometer "Membrana-2" ($< \lambda > = 3$ Å) has achieved the same efficiency only at $P(^3\text{He}) = 4$ bar, Fig. 2. To keep the detector efficiency stable for a long time and to make it insensitive to possible gas leakage from the gas volume, the working pressure of the ^{3}He gas was chosen on the plateau, indicated by arrows in Fig. 2.

2.4. Design of the electrodes

The neutron detectors are closed in a sealed gas-filled volume. To guarantee long-term detector performance and to prevent degradation of the energy resolution, it is necessary to maintain a high level of the gas mixture purity. In other words, the detector must be fabricated from the materials which can be pumped to high vacuum and heated up to at least 100 °C. To minimize outgassing of the detector inner parts, we have developed a new technology of fabrication of the detector electrodes. Now, all electrodes are fabricated from quarts glass and are subject to high vacuum pumping and heating up to 130 °C. The properties of the deposited printed circuits are staying constant even after heating of the frame up to 150 °C. The wire soldering is done by a solder with the melting point at 280 °C. This technology has opened a way to improve the gas purity by several orders of magnitude. No glues are used in the detector construction.

The new technology has provided an increased lifetime and stable operation of the detectors since 2007 without refilling the gas.

3. Experimental results

3.1. Detector efficiency

To measure the detector efficiency, a reference proportional counter filled with the ^{3}He gas under 10 bar pressure intended for thermal neutron detection with the efficiency of about 100 % was used. Our detector of neutrons and the proportional counter were irradiated by a collimated neutron beam independently. The ratio of the counting rates demonstrated us that our detector has the efficiency about $\varepsilon = 70\ \%$, which is in good matching with the results of calculations (see section 2.3). The neutron beam flux density was $1.7 \times 10^4\ \text{s}^{-1}\text{cm}^{-2}$.

3.2. Differential nonlinearity

The differential nonlinearity is the derivative dx_m/dx of the position calibration curve $x_m = f(x)$, where x_m is the measured neutron position and x is the true position. A measure of the differential nonlinearity is prompted by the flat response of a uniform illumination spectrum. Any nonuniformity of the detector efficiency is also encompassed by this spectrum. Figure 3 shows a uniform illumination spectrum along the anode wires (X-axis) obtained with a wide beam of thermal neutrons. The differential nonlinearity of this measurement is very small and does not exceed $\pm 7\%$. This parameter is very sensitive to boundary discontinuities between the two multi-pin connectors transferring the signals from the cathode strips. There was no indication of discontinuities at the section boundaries.
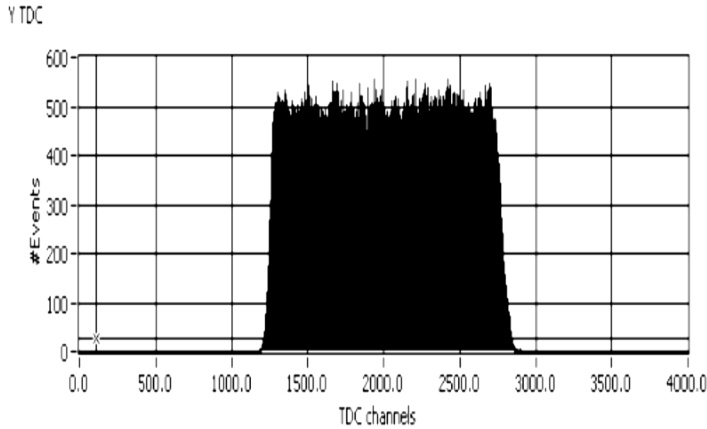

Fig. 3. Uniform illumination spectrum along the fine resolution axis (parallel to the anode wires)

3.3. Position resolution

We point out three more important parameters, which are directly related to the detector position resolution: the ranges of particles produced in the reaction (determining the physical limit of the detector position resolution); the geometrical structure of the MWPC, and the intrinsic resolution of the detector.

3.3.1. The range of primary particles

The physical limit of the detector position resolution is determined by the particle ranges from reaction (1) and their ionization losses. The proton and the triton are emitted in opposite directions from the point of the nuclear reaction, the emission being isotropic. The centroid of the ionization charge is displaced with respect to the point of the nuclear reaction due to different ionization losses of protons and tritons. The loci of the centroids for many neutrons are uniformly distributed on the surface of a sphere. The resulting probability distribution along any axis is rectangular. According to Ref. [1], the spheroid diameter is $D_{sph} = 0.7 \times R_p$, where R_p is the proton range.

The gas ^{3}He has low stopping power, and that is why CF_4 was used as a stopping gas to reduce the particle ranges. It localizes the electron avalanche near the anode wire in the point of its formation, and it has good quenching properties.

The position resolution of the detector is limited to D_{sph}, it is determined by the pressure $P(CF_4)$ of CF_4:

$$D_{sph} = 0.7 \times R_p \approx 2.8 \text{ mm} / P(CF_4) \text{ [bar]}. \tag{3}$$

So, the physical limit for the space resolution will be about 1.4 mm under the CF_4 pressure of 2 bar.

3.3.2. Readout method

The cathode strip Delay Line (DL) readout method was chosen to acquire the signals from the MWPC. It provides a high position precision and high integral counting capability (limited by the DL length, typically $T_{DL} < 1 \text{ μs}$) with the minimum number of electronic channels – only five.

The induced pulses come from the ends of a DL to a charge-sensitive PreAmplifier (PA), Fig. 4. The zero-crossing method was used to fix the signal arrival time to the PA. The time delay between the arrival of signals to the PAs was determined by the coordinate of the electron avalanche

$$x = \left(1 - \frac{t_2 - t_1}{T_{DL}}\right)\frac{L_{det}}{2}.$$

(4)

Here t_1 and t_2 are the times of arrival of signals at the ends of the DL, T_{DL} is the time length of the DL (ns), L_{det} is the geometric length of the cathode sensitive area along the coordinate X.

The structure of the MWPC and the readout method determine the measurement of coordinates. The coordinate spectrum along the X-axis (perpendicular to the anode wires) is discrete. The position resolution along the X coordinate ($FWHM_X$) is determined by the anode pitch S if the condition $D_{sph} < S$ is satisfied. The coordinate spectrum along the Y-axis (parallel to the anode wires) is continuous. The position resolution along the coordinate Y ($FWHM_Y$) does not depend on the anode pitch. It is determined by the value D_{sph} and the intrinsic resolution of the detector ($FWHM_{int}$):

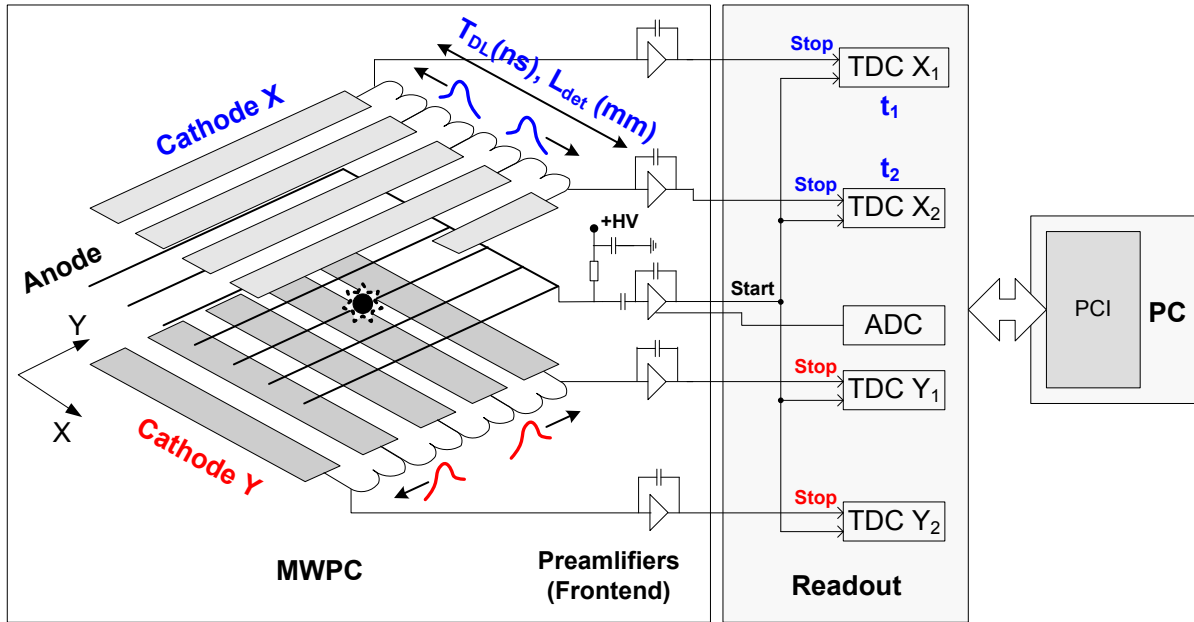$$FWHM_Y = \sqrt{D_{sph}^2 + FWHM_{int}^2}.$$

(5)

Fig. 4. Scheme of information readout from the MWPC. The cathode strips with a DL ($Z = 100$ Ohm), cathode preamplifiers (PAs with the input impedance $R_{in} = 100$ Ohm), Time-to-Digital Converters (TDCs), Analog-to-Digital Converters (ADCs), and the computer (PC) with a PCI-interface card are shown

The intrinsic resolution of the MWPC is determined by its design, by induced charge amplitudes, by the signal transmission quality of the DL, and by the noise level of the front-end electronics. In practice, the intrinsic position resolution $FWHM_{int}$ is limited by the noise generated in the termination of the DL with the PA:

$$FWHM_{int} \cong \frac{1}{\theta}\frac{e_n}{ZQ_c}\sqrt{\tau}.$$

(6)

Here $\theta = T_{DL}/\tau$ is the "quality" factor of the DL, τ is the dispersion of a signal in the DL, e_n is the noise spectral density ($V/Hz^{1/2}$).

To achieve the best physical parameters of the detectors, it was necessary to reach the required intrinsic resolution at the minimal gas gain. This regime is characterized by a lower level of the high voltage noise of the MWPC, a higher level of the gas gain uniformity and a higher amplitude resolution.

The designs of the DL and preamplifiers were refined in the detector prototype. In order to reach the value $\mathrm{FWHM_{int}} \leq 1$ mm, the impedance of the DL was chosen as high as possible, $Z = 100$ Ohm. To minimize the electronic noise, the input impedance of the cathode preamplifiers was chosen the same as the DL impedance $R_{in} = Z$ (the "electronic cooling" mode). In the result, the intrinsic resolution of the detector has reached the value $\mathrm{FWHM_{int}}t \leq 1$ mm at the gas gain $M \geq 130$ and $\mathrm{FWHM_{int}} = 0.5$ mm at $M = 200$.

3.3.3. Position readout in the direction perpendicular to the anode wires (*Y*-axis)

As one can see from the differential nonlinearity presented in Fig. 3, the uniform illuminated spectrum has a flat response, and no edge effects in this spectrum are observed, which usually manifest themselves as a rise of the local intensity at the spectrum edges. This means that the absolute position error in the *X*-direction is small.

Figure 5 shows the uniform illumination spectrum as seen in the *Y*-direction. One can see good shaped independent peaks with the modulation period of the anode wire spacing. Because the peak positions are determined by the gas avalanches surrounding the anode wires, it allows us to conclude that the integral nonlinearity along the *Y*-direction is less than 0.4 % (this is the measured absolute position error).

Generally speaking, it is possible to state that the absolute position error in both *X*- and *Y*-directions is small and considerably smaller than the space resolution determined by physical reasons.

It is essential to note that the width (FWHM) of these peaks means the real (intrinsic) resolution of the detector, which is affected by the electronic noise, the DL quality, the electric field structure, *etc*. The obtained results are presented in Fig. 6. As one can see, the intrinsic resolution of the detector is 0.6 mm, which is several times better than the physical limit D_{sph}.
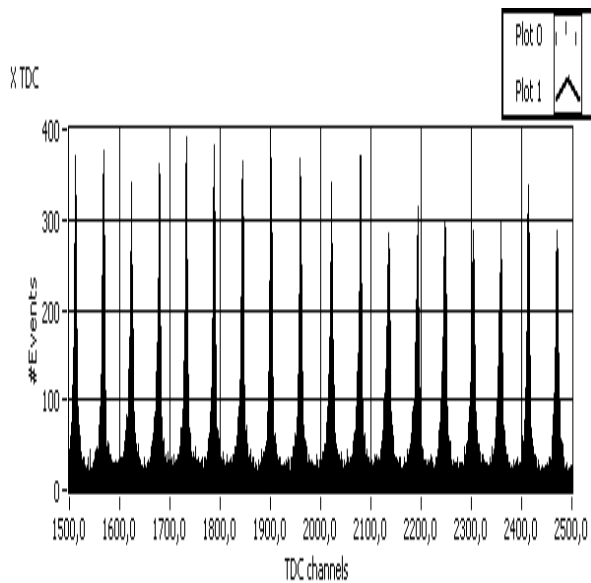
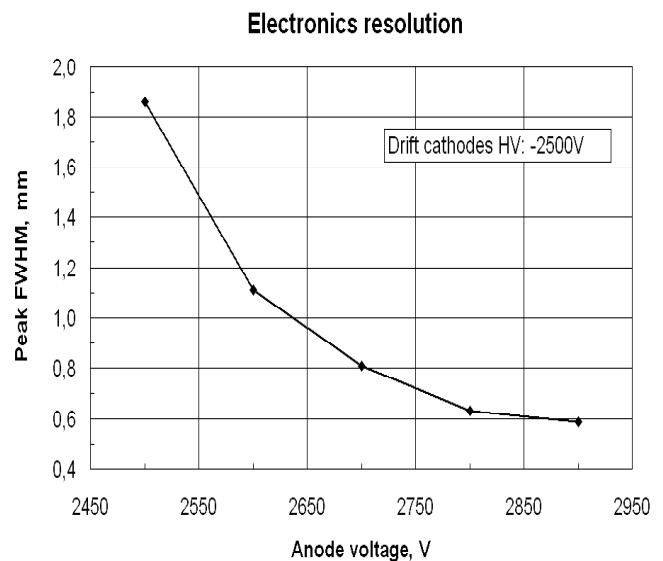**Fig. 5.** Uniform illumination spectrum along the discrete axis (perpendicular to the anode wires)

Fig. 6. Intrinsic resolution of the detector *vs* high voltage

3.3.4. Position resolution in the direction along the anode wires (*X*-axis)

To measure the space resolution, the detector was irradiated by a narrow neutron beam with its width being discretely changed in the range from 4.0 to 0.5 mm by cadmium collimators. A typical view of the obtained spectra is shown in Fig. 7. As one can see from the obtained data in Fig. 8, the detector spatial resolution is about FWHM = 1.5 mm.

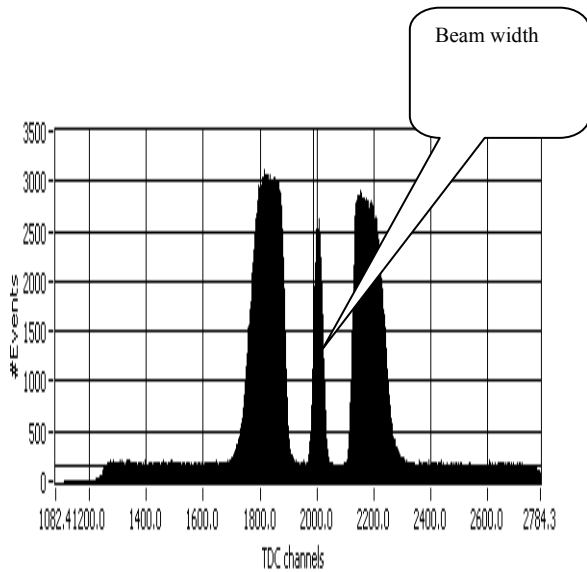This is in good matching with the expected neutron resolution.

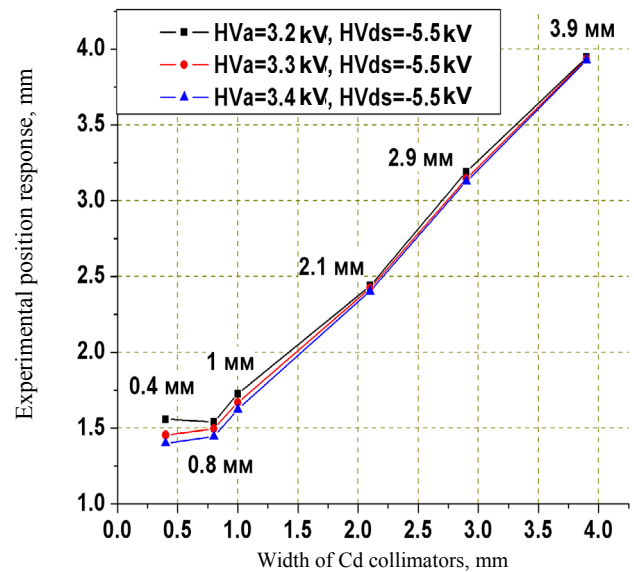**Fig. 7.** Experimental method of the neutron position response measurement along the fine resolution axis

Fig. 8. Results of measurements of the spatial resolution of the detector

3.4. Energy spectra

The shape of the amplitude spectra is an important characteristic of the neutron detector. It is determined by the gas composition and its purity, the gas pressure, the gas gain and its uniformity along the detector window, the applied anode and cathode voltages.

3.4.1. Amplitude spectra of the neutron detectors and the standard neutron counter

The pulse height spectra dependence on the anode high voltage and the electric field in the drift regions was investigated. It was shown that the neutron detector spectra (Fig. 9b) are very similar to those obtained with the reference proportional counter with the gas pressure of 10 bar and look like a "dark body" for thermal neutrons, Fig. 9a.

The energy spectrum has a well-defined peak corresponding to the energy released in reaction (1). There are bumps corresponding to the energies of the proton (573 keV) and the triton (191 keV). Some distinctions are due to the fact that the detectors were filled with different gas mixtures (various concentrations of ^{3}He and CF_4 in the gas mixtures and different pressures) and that the 2D-detector is a multi-wire detector consisting of several hundred of anode wires.
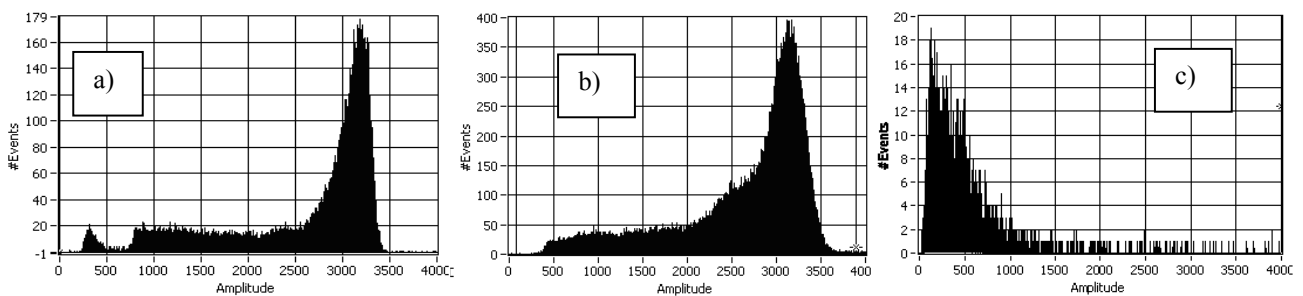

Fig. 9. Amplitude spectra measured with the neutron detectors. a – standard neutron counter SNM-50, high voltage was 2.0 kV; b – neutron detector, anode high voltage is $H_A = 2.6$ kV, cathode high voltage $HV_{DS} = -2.5$ kV. The intrinsic noise of the detector was rejected by the PA threshold; c – intrinsic noise of the neutron detector. The PA threshold is about zero

The intrinsic noise and the background spectrum of the neutron detectors are located in the low-amplitude part of the spectrum (Fig. 9c). Therefore, a correct choice of the events discrimination threshold can provide a minimal level of noise, keeping the neutron efficiency value constant. It corresponds approximately to the triton energy E_T =191 keV or ¼ of the peak amplitude of the total energy.

3.4.2. Amplitude spectra and background discrimination

An investigation of γ-sensitivity of the detectors has shown that amplitudes of events caused by registration of γ-rays are rather small. Therefore, if necessary, a rejection of low-amplitude events can provide very low γ-sensitivity of the detectors, $\varepsilon_\gamma \approx 1.8 \times 10^{-8}$ with small reduction of the neutron detection efficiency, < 5 % (Fig. 10). This feature allows to effectively register thermal neutrons in a high background of γ-quanta.
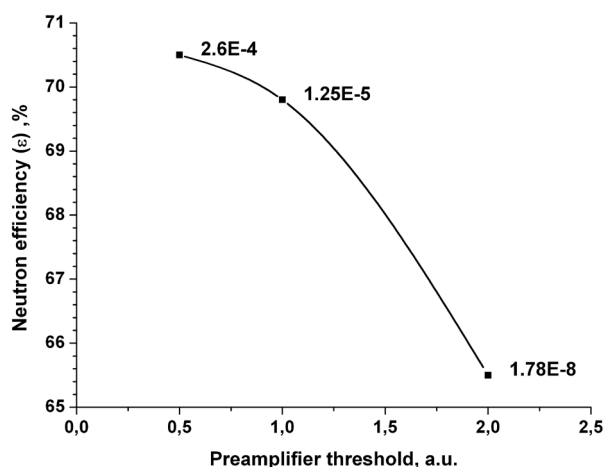

Fig. 10. Neutron- and γ-sensitivity of the detector with the entrance window 200 × 200 mm^2 *vs* the preamplifier threshold. The γ-source ^{137}Cs: A = 80 MBq, E_γ = 0.662 MeV

3.4.3. Gas purity control

Insufficient purity of the working gas dramatically affects the operation of the detector. It leads to violation of the operating parameters and makes impossible to ensure the correct functioning of the detector. Therefore, at the stage of the gas filling of each detector, the amplitude spectra were measured with the proportional counter SNM-50. Typical spectra are shown in Fig. 11.
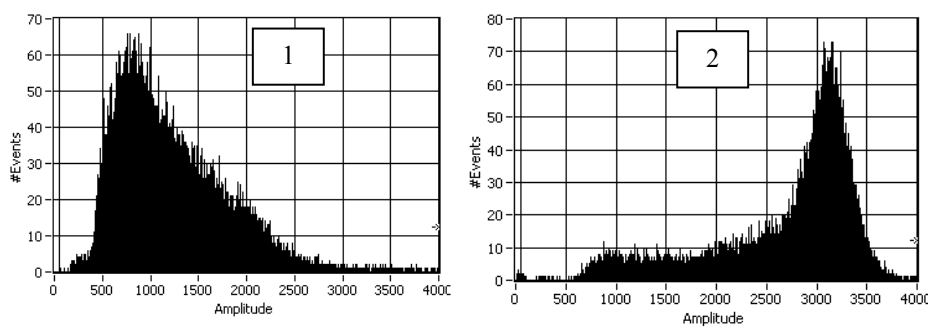

Fig. 11. Amplitude spectra measured by the neutron counter SNM-50 filled with the investigated gas. 1 – before ^{3}He cleaning. Gas mixture: (4 bar ^{3}He + + 100–300 ppm of O_2) + 2 bar CF_4; 2 – after ^{3}He cleaning. Gas mixture: 4 bar ^{3}He + 2 bar CF_4

4. Conclusion

Thermal neutron detectors for the diffractometers "Vector" and "Membrana-2" have been designed, constructed and successfully tested [4]. All required parameters have been achieved, as in Table 2. These detectors were successfully used in neutron diffraction experiments at the reactor VVR-M of PNPI.